Osteoarthritis leads to more contractile and protrusive chondrocytes when cultured in 3D degradable hydrogels

Maxim Vovchenko[1,2*], Nele Vaes[1*], Jorge Barrasa-Fano[1], Apeksha Shapeti[1], Rocio Castro Vinuelas[34], Laurens Kimps[1], Christ Glorieux[2], Ilse Jonkers[345], Hans Van Oosterwyck[16#]

[1] Biomechanics Section, Department of Mechanical Engineering, KU Leuven, Leuven, Belgium
[2] Laboratory for Soft Matter and Biophysics, Department of Physics and Astronomy, KU Leuven, Leuven, Belgium
[3] Human Movement Biomechanics Research Group, Department of Movement Sciences, KU Leuven, Leuven, Belgium
[4] Skeletal Biology and Engineering Research Center, Department of Development and Regeneration, KU Leuven, Leuven, Belgium.
[5] Institute for Physics-Based Modeling for In Silico Health, KU Leuven, Leuven, Belgium
[6] Prometheus Division of Skeletal Tissue Engineering, KU Leuven, Leuven, Belgium
[*] equal contribution
[#] correspondence: hans.vanoosterwyck@kuleuven.be

Abstract

Osteoarthritis (OA) significantly influences chondrocyte behavior, yet its impact on active cell-generated forces, a key indicator of cell-matrix interaction, remains poorly understood. In this study, we used traction force microscopy (TFM) and immunostaining to explore how culture dimensionality (2D versus 3D) affects cell phenotype and contractile dynamics in human articular chondrocytes from both OA and non-OA patients. Our findings reveal that OA alters key proteins involved in force exertion and transmission across both culture dimensionalities, with pronounced phenotypical differences observed in the 3D environment. While OA does not affect chondrocyte-generated tractions in 2D cultures, it enhances contractility in 3D degradable hydrogels, correlating with increased protrusive activity, higher actomyosin engagement, and altered extracellular matrix remodeling. These findings show that the 3D environment highlights OA-related changes in chondrocyte mechanobiology, emphasizing the necessity of considering culture dimensionality and degradability in OA research.

Introduction

Osteoarthritis is a common degenerative joint disease characterized by the breakdown of articular cartilage, leading to pain, stiffness, and reduced mobility. A fundamental aspect of OA is the alteration in the behavior and characteristics of chondrocytes, cartilage cells responsible for maintaining cartilage health. Research has shown that OA chondrocytes undergo significant changes, including hypertrophy and altered expression of specific markers, which contribute to the disease progression[1]. Understanding these cellular changes is crucial for developing targeted therapies and interventions.

Mechanical loading is essential for normal cartilage maintenance – moderate, cyclic loads is essential to cartilage homeostasis, among others by promoting the synthesis of cartilage extracellular and pericellular matrix components. However, abnormal mechanical stimuli can impair chondrocyte function and contribute to OA progression. Insufficient mechanical stimulation, such as prolonged joint immobilization, deprives chondrocytes of necessary mechanical cues and nutrients (which transport is promoted by pressure gradient induced interstitial fluid flow), leading to phenotype change or even cell death and matrix loss [2]. On the other end, excessive mechanical stress can injure cartilage and initiate degenerative changes. In fact, overloading of

joints is a known risk factor for OA pathogenesis: excessive mechanical stress on cartilage induces cellular damage and accelerates chondrocyte senescence, ultimately promoting cartilage degeneration [3]. Chondrocytes subjected to injurious loads upregulate catabolic enzymes such as MMPs and pro-inflammatory mediators, shifting the tissue balance toward breakdown. Over time, chronic mechanical overloading fosters an OA-like phenotype in chondrocytes, whereas a balanced mechanical environment is key to preserving their normal function.

One of the key components in studying OA chondrocytes is mechanotransduction—the process by which cells sense and respond to mechanical stimuli from their environment. Key structures at the cell surface mediate this process: the pericellular matrix (PCM) transmits forces to mechanoreceptors on the chondrocyte membrane, including stretch-activated ion channels, the primary cilium, and integrin receptors [4]. These receptors sense mechanical deformation and initiate intracellular cascades that ultimately regulate gene expression, allowing chondrocytes to adapt to changing mechanical loads. The cytoskeleton plays a central role in this signaling. For example, integrins span the cell membrane and physically link the extracellular matrix to the intracellular actin cytoskeleton, creating a structural molecular mechanical network for force transmission between the extracellular and intracellular environment [5]. When mechanical forces are applied to cartilage, they are conducted through integrin–matrix connections into the cytoskeleton, resulting in cytoskeletal reorganization and activation of downstream signaling pathways. Thus, the organization of actin filaments and other cytoskeletal elements is dynamic in chondrocytes, realigning in response to mechanical stimuli as part of the cell's adaptive mechanotransduction mechanism.

Cell–matrix interactions, largely governed by integrin receptors, play a crucial role in chondrocyte mechanobiology and become dysregulated in OA. OA chondrocytes often exhibit altered integrin expression profiles that affect how these cells adhere to and sense the extracellular matrix (ECM). For instance, the integrins α1β1 and α3β1 are found at abnormally high levels in OA cartilage, which is thought to contribute to aberrant matrix remodeling and even promote a hypertrophic-like change in chondrocyte phenotype [4]. Such changes suggest that OA chondrocytes may attach more firmly or inappropriately to the altered cartilage matrix, potentially modifying force transmission. Moreover, integrin-mediated signaling in OA intersects with inflammatory pathways. Dysregulation of αV-class integrins (such as αVβ3 and αVβ5) has been shown to exacerbate joint inflammation and cartilage breakdown; conversely, blocking these integrins can reduce the production of key pro-inflammatory cytokines like IL-1β and TNF-α in cartilage [4]. These findings highlight integrins as critical modulators of both the biomechanical and biochemical environment in OA.

Pro-inflammatory cytokines present in OA joints (notably IL-1β and TNF-α) strongly influence chondrocyte actin dynamics. These cytokines activate Rho-family GTPase pathways (such as RhoA/ROCK), which in turn promote actin polymerization and the formation of extensive stress fibers in chondrocytes [6]. In vitro studies show that exposing chondrocytes to IL-1 can induce a dramatic reorganization of the actin cytoskeleton: treated cells develop prominent, thick stress fibers and a corresponding decrease in the ratio of monomeric (G-) to filamentous (F-) actin, indicating a shift toward an F-actin–rich phenotype. Such cytoskeletal changes are associated with more fibroblast-like behavior, which parallels the phenotype observed in OA cartilage. However, sustained inflammatory stimulation may eventually exhaust the cell's structural adaptability – prolonged exposure to IL-1β has been reported to disrupt the organization of the actin cytoskeleton and associated proteins, essentially leading to actin network disassembly in chondrocytes. Alterations in actin dynamics feed back into cell signaling: the excessive stress fiber formation enhances focal adhesion signaling and cell contraction, while cytoskeletal disassembly can impair mechanotransduction. Together, these inflammation-driven cytoskeletal perturbations contribute to OA progression by altering chondrocyte shape, mechanics, and gene expression in a way that favors cartilage breakdown.

Elevated fibronectin levels have been associated with ECM remodeling in OA, where altered fibronectin organization can influence cellular responses and matrix degradation [7], [8]. In OA chondrocytes, increased fibronectin deposition may act as a compensatory mechanism for impaired adhesion and signaling. However, elevated fibronectin levels can lead to the generation of fibronectin fragments through proteolytic cleavage by MMPs. These FN fragments activate signaling pathways, notably toll-like receptor-2 (TLR-2) and mitogen-activated protein kinase (MAPK), which further upregulate MMP expression, creating a feedback loop that enhances ECM degradation and contributes to cartilage deterioration.

The mechanical properties of the extracellular matrix are crucial for chondrocyte function and health, and changes in cartilage stiffness during osteoarthritis contribute to chondrocyte phenotypic shift [9]. Stiffer substrates tend to promote dedifferentiation, whereas softer substrates help maintain the chondrogenic phenotype, underscoring the importance of mimicking the natural ECM environment in culture conditions. Chondrocyte behavior differs markedly between two-dimensional (2D) and three-dimensional (3D) culture systems [10]. In 2D monolayer cultures on rigid plastic, chondrocytes spread out extensively [11], [12], forming actin stress fibers and focal adhesions that result in a fibroblast-like morphology and reduced expression of cartilage-specific markers, such as type II collagen and SOX9 [12], [13]. In contrast, 3D culture systems—such as pellet cultures, alginate beads, and collagen/PEG hydrogels—preserve a rounded cell morphology and a cortical actin cytoskeleton that more closely resembles in vivo cartilage, thereby supporting robust ECM production and maintenance of the chondrogenic phenotype [10], [14], [15]. Differences in cell shape between these culture conditions are closely linked to integrin-mediated interactions with the ECM [2]. In 2D, chondrocytes adhere via integrins to the rigid substrate, which alters their integrin profiles (with increased expression of subunits β1 and α2) and may drive dedifferentiation, whereas 3D cultures facilitate more physiological integrin signaling. Moreover, chondrocytes in 3D typically produce higher levels of glycosaminoglycans and type II collagen [15], while 2D cultures often shift toward a fibrocartilaginous phenotype with increased type I collagen synthesis [10], failing to capture the dynamic balance between ECM synthesis and degradation observed in vivo. Additionally, 2D culture leads to reduced chondrogenic gene expression and upregulation of hypertrophy markers, while 3D systems better preserve differentiation and amplify OA-associated catabolic and inflammatory responses, including elevated matrix metalloproteinase expression and cytokine release [16], [17]. Despite the simplicity of 2D culture, its limitations in replicating native chondrocyte environment conditions underscore the importance of 3D models for studying chondrocyte behavior in OA.

Previous studies have highlighted the effect of OA on actin organization (primarily for OA chondrocytes cultured on non-physiological 2D rigid substrates) and integrin expression (i.e at mRNA level). None of these studies have attempted to investigate the consequences of these OA-associated changes for active cell-generated forces. Such information is needed to better determine a chondrocyte's active cell mechanical state, which in turn is crucial for mechanotransduction and which would complement the existing (and abundant) literature on the role of external mechanical loading for healthy and OA chondrocyte phenotypes. Among the various methods that are available to measure active cellular forces, traction force microscopy (TFM) is the most established and versatile, in particular since it can be applied to 2D and 3D cell cultures, thereby also enabling to make comparisons between 2D and 3D. The latter is important, given the fact that culture dimensionality has an effect on chondrocyte and OA phenotypes and that in vitro studies often report on 2D culture experiments only. So far, there has been only three reports on the use of TFM for chondrocyte active force generation, both being limited to 2D TFM. Chen et al. [18] have demonstrated that TGF-β1 induces a stiffness dependent increase in traction forces and IL-1β induces a stiffness dependent decrease in traction forces. In a second study [19], they mechanically compressed chondrocytes and observed a decreased traction forces for vimentin disrupted cells, indicating the importance of the cytoskeleton in response to mechanical

loading. A study by Zhen et al. [20] demonstrated increased traction forces when subjecting chondrocytes to shear stress. Interestingly, this increase was lost when they silenced talin, an actin binding cytoskeletal protein located at focal adhesions, indicating the importance of a maintained cell-ECM coupling in response to mechanical loading. However, all experiments from these studies were done with healthy chondrocytes, so that up to now there is a complete lack of information on the effect of OA on chondrocyte force generation. Our study addresses this knowledge gap and applies 2D and 3D TFM to human chondrocytes harvested from non-OA and OA patients and cultured on 2D non-degradable and 3D degradable soft hydrogels. TFM measurements are complemented with fluorescence image-based quantification of cytoskeletal, adhesional and ECM proteins, so that chondrocyte traction data can be associated to key players of force exertion and transmission. Our results show that OA affects key proteins of force exertion and transmission for 2D and 3D cultures, but that these differences are dependent on culture dimensionality and degradability. While chondrocyte tractions are not affected by OA when cultured in 2D, they are when cultured in 3D, degradable hydrogel environments: OA chondrocytes are more contractile than non-OA chondrocytes, which can be associated to enhanced protrusive activity in such environments and which demonstrates an interplay between actin protrusion, degradation and contractility.

Results

OA chondrocytes are larger than healthy chondrocytes and show different actin distribution pattern along with increased matrix remodeling

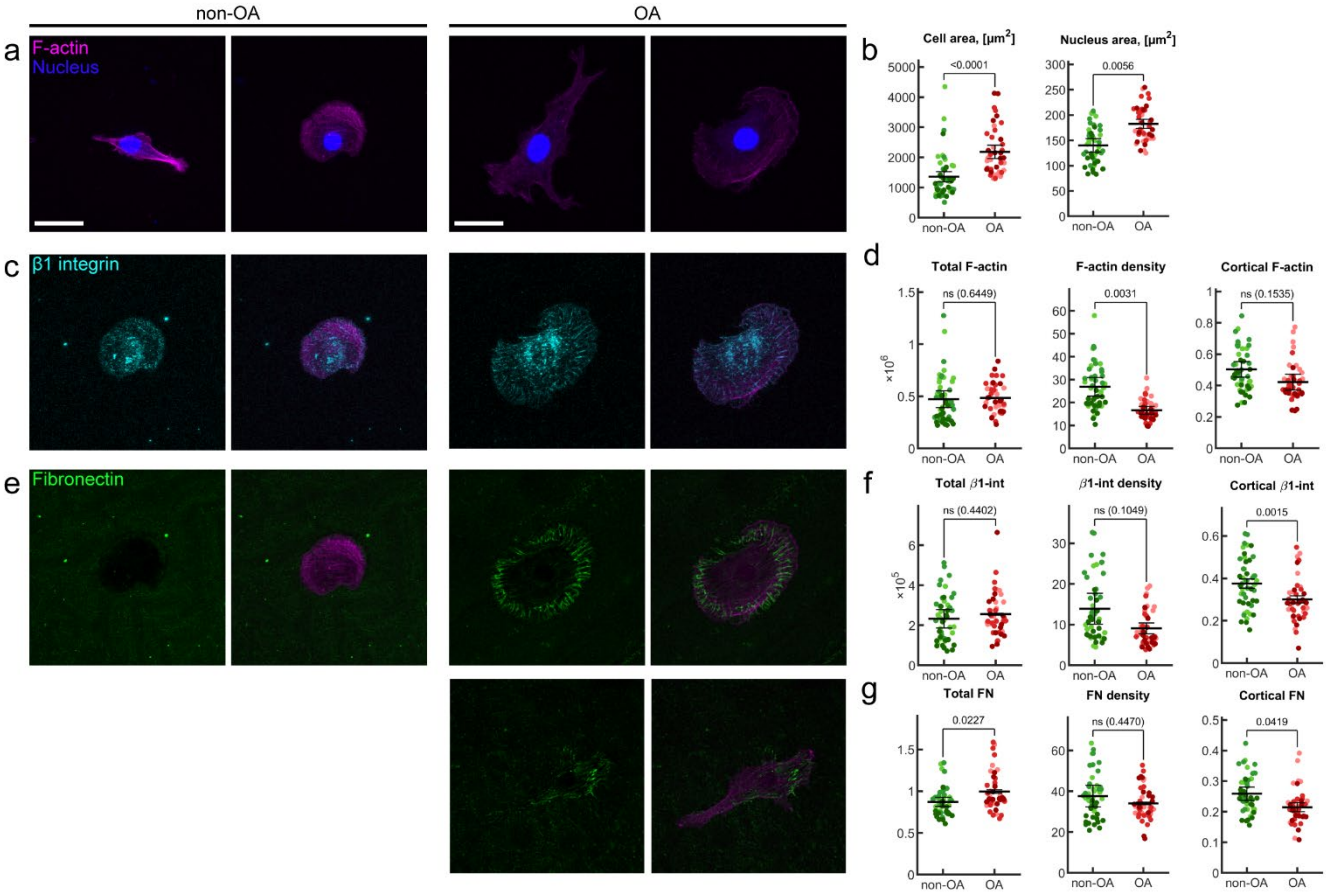

Figure 1. ***a*** *Maximum intensity projections of F-actin localization of two representative non-OA (healthy) and OA chondrocytes, 24h after seeding on PAA hydrogel.* ***b*** *Cell and nuclear area morphological metrics, representative for cell and nuclear volumes.* ***c*** *Maximum projection of β1 integrin expression (cyan) and overlay with F-actin (magenta) for a representative non-OA and OA chondrocyte.* ***d*** *Quantification of F-actin expression: Total F-actin intensity of a cell, Total F-actin intensity normalized by cell area, ratio of F-actin present in the cortex normalized*

by the total F-actin intensity. ***e*** *Fibronectin expression (green) and overlay with F-actin (magenta) for a representative non-OA and two representative OA chondrocytes.* ***f*** *Quantification of β1 integrin expression: Total β1 integrin intensity of a cell, Total β1 integrin intensity normalized by cell area, ratio of β1 integrin present in the cortex normalized by the total β1 integrin intensity.* ***g*** *Fibronectin intensity of a cell normalized to background signal, fibronectin intensity normalized by cell area, ratio of fibronectin present in the cortex normalized by the fibronectin intensity. All statistical comparisons used generalized linear mixed-effects models to account for the nested structure of the data. Error bars represent SEM, scalebars are 30 μm. Each green and red hue in the graph represents a different patient (N=3 for each condition), each dot represents the value for one cell (n≥15 for every patient).We cultured primary human articular chondrocytes isolated from hip joints of non-OA affected donors and OA patients on soft (4.5 kPa) 2D fibronectin-coated non-degradable polyacrylamide (PAA) gels. A soft substrate was selected to avoid inducing a catabolic state in non-OA cells, as stiff matrices are known to shift chondrocyte homeostasis towards catabolism [21], similar to what is observed in OA cells. Sparse cell seeding, mirroring the natural sparse in vivo distribution of chondrocytes, ensured individual analysis of OA-specific phenotypic changes in cell morphology, cytoskeletal organization, and cell-matrix adhesion components.*

In osteoarthritic cartilage, chondrocytes become hypertrophic, characterized by increased cell size and expression of type X collagen (COL10A1) and MMP-13, due to aberrant differentiation driven by inflammatory cytokines (e.g., IL-1β, TNF-α), matrix degradation, and altered mechanotransduction [6], [22]. In OA chondrocytes, the cell phenotype is characterized by increased levels of F-actin, β1 integrin, and fibronectin. To determine if these phenotypic alterations persist when OA chondrocytes are cultured on soft matrices, we performed immunostaining for these molecules after 24 hours of culture.

OA chondrocytes exhibited a significantly larger projected cell area compared to non-OA cells (Fig. 1a, 1b), consistent with cellular hypertrophy linked to OA progression [22]. To determine whether this morphological shift is coupled with cytoskeletal reorganization, F-actin levels were quantified (Fig. 1d). While total F-actin content did not differ between groups, OA cells displayed reduced F-actin density, which was inversely correlated with their increased spreading. This suggests that the cellular enlargement in OA occurs without proportional cytoskeletal reinforcement. Additionally, while not statistically significant, there was a noticeable trend suggesting that non-OA cells maintained cortical actin localization, whereas OA cells exhibited a more homogeneous cytoplasmic distribution of actin.

Further, we aimed to study nuclear morphology in OA chondrocytes to see if there any alterations that might be caused by observed altered cytoskeleton or ECM cues. Alterations in nuclear shape and organization have been linked to disrupted mechanotransduction, altered gene expression, and cellular dysfunction in OA [23]. Morphologically, non-OA and OA chondrocytes exhibited no significant differences in global shape characteristics, including eccentricity, solidity, or circularity, indicating preserved overall cellular morphology (Fig. S1). However, significant difference emerged at the nuclear level: looking at DAPI-stained nuclei and quantifying nuclear morphology, we noticed that OA cells exhibited a larger nuclear area in accordance with [24] (Fig. 1b). This change may reflect nuclear deformation caused by cell flattening, which may impair cell transcriptional regulation shifting altering homeostasis [2].

Given that integrin dysfunction has been implicated in OA progression, we wanted to investigate whether OA chondrocytes exhibit altered integrin localization, potentially contributing to impaired cell-matrix signaling and cartilage degradation. An analysis of β1 integrin (Fig. 1c, 1f) revealed that, despite similar total expression levels between OA and non-OA chondrocytes, integrin density indicated a decreasing trend in OA cells. This suggests that OA chondrocytes may form fewer focal adhesion complexes per unit of area. While [25] observed increased total β1 integrin expression in OA chondrocytes using immunoprecipitation and mRNA analysis, their findings do not necessarily translate in similar differences at protein level and reflect the overall production of integrins, including those that are intracellular or newly synthesized. In contrast, our immunostaining-based approach

highlights integrin localization, surface availability, and clustering at adhesion sites. The discrepancy suggests that although OA chondrocytes may produce more integrins, they fail to properly traffic and organize them into functional adhesion complexes, particularly on soft substrates.

To further study cell-ECM interaction, we looked at fibronectin deposition due to its important role in maintaining cartilage integrity and regulating chondrocyte behavior. In OA, fibronectin levels are often elevated, and its organization within the ECM is disrupted, potentially influencing cell adhesion, signaling, and matrix remodeling [8]. Supporting this, our findings showed that fibronectin deposition was significantly increased in OA chondrocytes (Fig. 1e, 1g), exhibiting higher total fibronectin intensity, while fibronectin density was similar for OA and non-OA, indicating an increase in total fibronectin correlated to the increased cell area observed in OA. Cortical distribution of fibronectin was decreased compared to non-OA.

Notably, in OA chondrocytes, fibronectin was frequently organized into distinct strand-like patterns (Fig. 1e), reflecting active ECM remodeling and similar to the observations from [7]. This organization was not commonly seen in healthy cells: 56% of OA chondrocytes exhibited this pattern, compared to only 16% of non-OA cells (Fig. 1e), highlighting a significant difference in fibronectin organization between the two groups. This altered fibronectin distribution may serve as a compensatory response to impaired adhesion or, alternatively, as a driver of pathological signaling, given that excessive fibronectin fibrillogenesis has been linked to catabolic pathways in OA [26]

Collectively, these results indicate that in a soft 2D matrix environment, OA chondrocytes exhibit distinct alterations in cell spreading, cytoskeletal organization, and ECM remodeling that could underlie the pathological progression of osteoarthritis.

OA chondrocytes show no difference in force exertion patterns compared to healthy chondrocytes

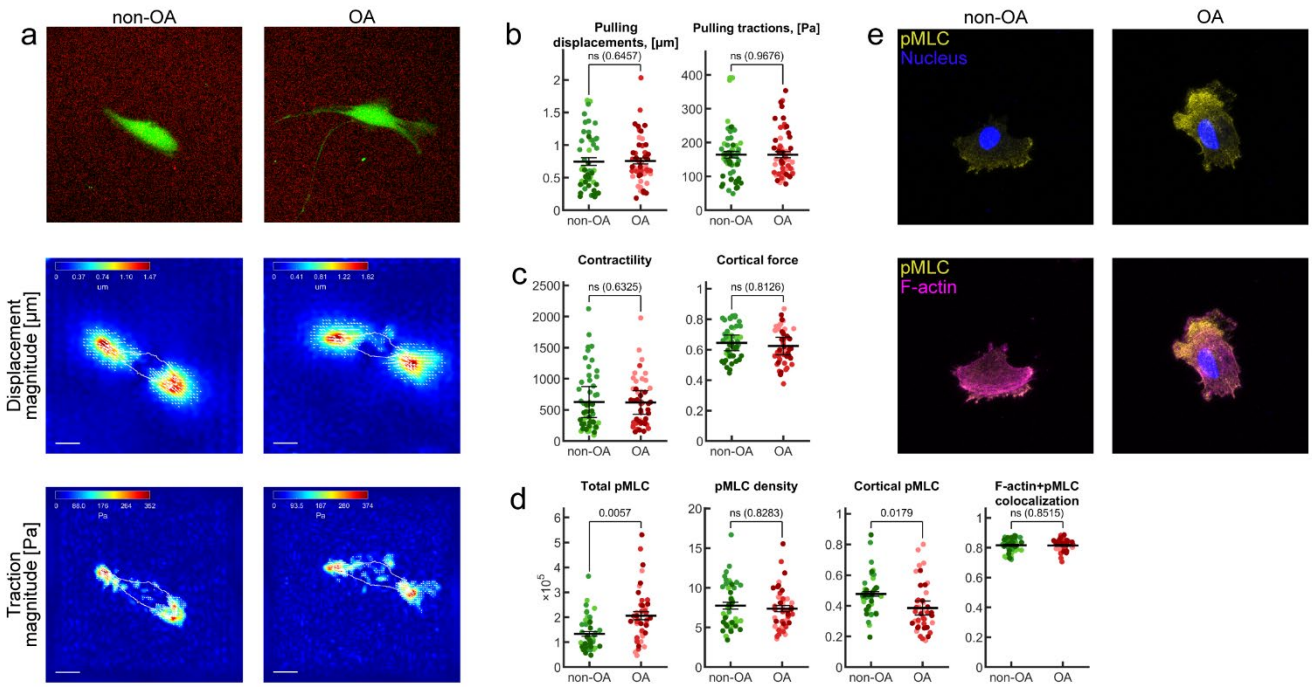

Figure 2. ***a*** *2D TFM results illustration. (top) Representative maximum projected images of beads (red) and chondrocyte (green) for one non-OA and one OA chondrocyte. (middle) Corresponding displacement magnitude renders. (bottom)* Corresponding traction force magnitude renders. ***b*** *Quantification of the 99th percentile bead*

displacement magnitude [µm] and the 99th percentile traction force magnitude [Pa]. ***c*** *Quantification of contractility, sum of the 95th percentile traction force vectors projected on the axis connecting the corresponding pixel to the cell centroid. Quantification of cortical force as the ratio of traction forces in the cortex, normalized by the total traction force.* ***d*** *Quantification of pMLC expression: total pMLC intensity of a cell, total pMLC intensity normalized by the cell area, pMLC intensity in the cell cortex normalized by total pMLC intensity, colocalization of F-actin with pMLC.* ***e*** *Maximum intensity projection of pMLC (yellow) and overlay with F-actin (magenta) for a representative non-OA and OA chondrocyte. All statistical comparisons used generalized linear mixed-effects models to account for the nested structure of the data. Error bars represent SEM, scalebars are 30 µm. Each green and red hue in the graph represents a different patient (N=3 for each condition), each dot represents the value for one cell (n≥15 for every patient).*

Since we observed alterations in cell area, cytoskeleton and components of the cell-ECM coupling, such as β1 integrin and fibronectin for OA chondrocytes, we wondered how these alterations affect the force generation capacity of OA chondrocytes. To evaluate this, we performed a series of 2D traction force microscopy (TFM) experiments on primary human articular chondrocytes isolated from hip joints of healthy donors and OA patients. Cells were seeded on soft (4.5 kPa) fibronectin-coated PAA gels embedded with 200 nm fluorescent beads (Fig. 2a). For each cell, two sets of Z-stack images were acquired: one representing the “stressed” state, captured 24 hours after cell seeding, when the chondrocytes had adhered and deformed the gel surface, and a second representing the “relaxed” state, obtained 15 minutes after treatment with a droplet of 5% sodium dodecyl sulfate (SDS) that washed away the cells and relaxed the substrate. Bead displacements between these states were measured and, together with the known mechanical properties of the gel, used to calculate cellular traction forces.

Our TFM analysis revealed no significant differences in cell-generated bead displacements or traction forces between non-OA and OA chondrocytes (Fig. 2b). Additionally, we observed no differences when looking at contractility, a global metric for the capacity of the cell to exert pulling forces (Fig. 2c). Since we observed decreased cortical distribution of the actin cytoskeleton, β1 integrin and fibronectin for OA chondrocytes, we wondered how these alterations translated into traction force distribution. Interestingly, these differences in components of cell-ECM coupling did not result in different cortical traction distribution (Fig. 2c). Previously, we observed that OA cells displayed an increased cell area and a reduced F-actin density and lower β1 integrin density. These alterations would typically be expected to weaken the efficiency of force transmission. The fact that overall traction remains unaltered suggests that OA chondrocytes may compensate for these structural deficits by reorganizing their contractile machinery, thereby maintaining effective force generation despite a sparser actin network.

Supporting this idea, immunostaining revealed that OA cells exhibit a higher total phosphorylated myosin light chain (pMLC) level compared to non-OA cells, and pMLC density was comparable between groups (Fig. 2d, 2e). This comparison was performed as a molecular readout of contractile activity, given that pMLC is essential for actomyosin contraction. Notably, OA cells displayed reduced pMLC accumulation at the cell cortex (Fig. 2d)—a finding consistent with our earlier observation of diminished cortical F-actin. The measured degree of actin–pMLC colocalization was similar in both cell types (Fig. 2d), underscoring that the essential coupling between actin filaments and contractile elements is preserved in OA chondrocytes cultured on a soft 2D substrate. These findings could explain the maintained global cell-generated traction force level in OA cells.

OA cells in 3D are morphologically different from healthy chondrocytes

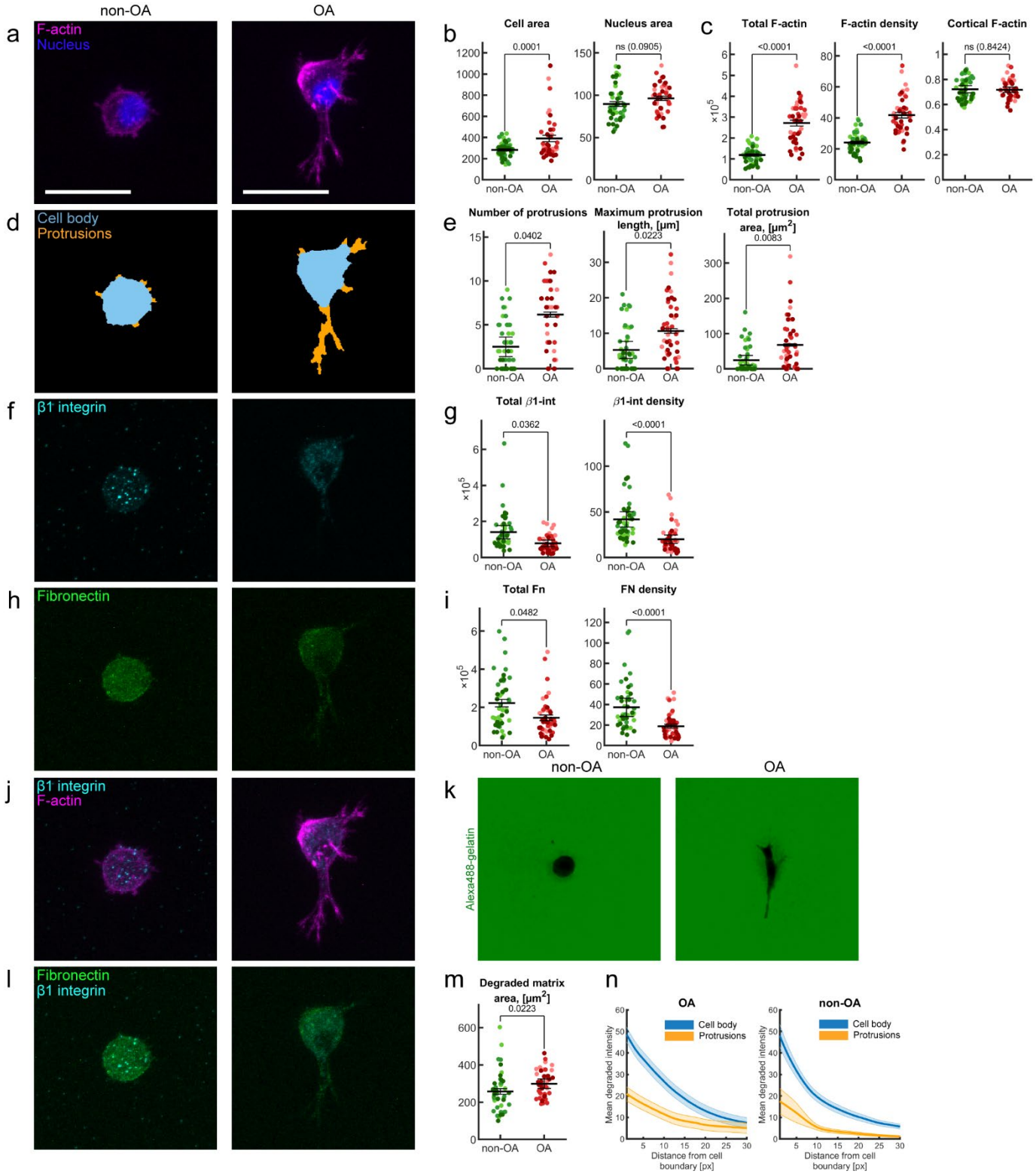

Figure 3. ***a*** *Maximum intensity projection of F-actin expression (magenta) and Nucleus (blue) for a representative non-OA and OA chondrocyte.* ***b*** *Cell area morphological metric, representative for cell volume. Nuclear area morphological metric, representative for nuclear volume.* ***c*** *Quantification of F-actin expression: Total F-actin intensity for a cell, total F-actin intensity normalized by cell area, F-actin cortex computed as the F-actin in the cortex normalized by the total F-actin intensity.* ***d*** *Automatic segmentation of cell body (light blue) and protrusions (orange) for corresponding non-OA and OA chondrocyte.* ***e*** *Protrusion quantification: Number of protrusions, Maximum protrusion length per cell and Total protrusion area.* ***f*** *Maximum intensity projection of β1 integrin*

expression (cyan) for a representative non-OA and OA chondrocyte. ***g*** *Quantification of β1 integrin expression: Total β1 integrin intensity for a cell, total β1 integrin intensity normalized by cell area.* ***h*** *Maximum intensity projection of fibronectin intensity for a representative non-OA and OA chondrocyte.* ***i*** *Quantification of fibronectin expression: Total fibronectin intensity for a cell, total fibronectin intensity normalized by cell area.* ***j*** *Overlay of maximum projected F-actin (magenta) with β1 integrin (cyan).* ***k*** *Minimum intensity projections of fluorescently labeled gelatin degraded by a representative non-OA and OA chondrocyte.* ***l*** *Overlay of maximum projected fibronectin (green) and β1 integrin (cyan) for representative non-OA and OA chondrocytes.* ***m*** *Quantification of total degraded matrix area using the degradation assay.* ***n*** *Mean degradation around cell body (blue) and protrusions (orange) for increasing distance away from cell boundary (in pixels). All statistical comparisons used generalized linear mixed-effects models to account for the nested structure of the data. Error bars represent SEM, scalebars are 30 μm. Each green and red hue in the graph represents a different patient (N=3 for each condition), each dot represents the value for one cell (n≥15 for every patient).To determine whether the observations made when culturing cells on a 2D PAA substrate hold true in a more physiologically relevant 3D environment, we encapsulated primary human articular chondrocytes from healthy donors and OA patients in a degradable PEG hydrogel. This hydrogel was engineered to include MMP-cleavable peptides (targeting MMP-1, MMP-2, MMP-3) and functionalized with RGD peptides to facilitate cell–ECM binding. Cells were seeded within the gel and cultured for 24 hours prior to fixation and immunostaining. All 3D image stacks were analyzed using maximum Z-projection method.*

Consistent with our findings in 2D culture, in 3D environment OA chondrocytes exhibited a significantly larger cell area (indicative of increased cell volume) compared to non-OA cells (Fig. 3b), while nuclear size, cell solidity, cell eccentricity and cell circularity remained unchanged (Fig. S2). Additionally, OA cells displayed a more protrusive phenotype characterised by higher number of cellular protrusions, along with increased protrusion length and area (Fig. 3d, 3e), underscoring an altered cytoskeletal organization.

To determine whether OA-related morphological changes are coupled with cytoskeletal remodeling, we further quantified F-actin levels and localization. In contrast to our 2D findings, OA chondrocytes exhibited both significantly higher total F-actin levels and density compared to non-OA chondrocytes (Fig. 3c, 3d). This increase in actin polymerization appears to be independent of the cell volume enlargement, reflecting an intrinsic upregulation of the actin network in OA cells in a 3D environment. Interestingly, despite these differences in total F-actin levels, cortical F-actin distribution remained comparable between OA and non-OA cells (Fig. 3c). This suggests that while intracellular actin polymerization is enhanced in OA chondrocytes, the overall organization of the cortical cytoskeleton is preserved and not decreased as it is for 2D case.

Integrin-mediated adhesion is critical for chondrocyte function, and dysregulation of integrin signaling has been implicated in OA progression. Despite their larger cell volume, OA chondrocytes in a 3D environment exhibited significantly lower total β1 integrin levels, and, consistent with our 2D findings, β1 integrin density was also decreased in comparison to healthy cells (Fig. 3f, 3g). Although this finding contrasts with previous reports of increased β1 integrin gene expression in OA [12, R. F. Loeser, 2014, DOI.], our nonspecific integrin staining—unable to distinguish between different α-units—and the short culture period may account for this discrepancy. In contrast to our 2D results, OA chondrocytes in 3D culture exhibited significantly lower total fibronectin deposition, both in terms of total amount and density (Fig. 3h, 3i). The decrease in fibronectin levels suggests that increased matrix breakdown in OA is coupled with impaired ECM deposition.

To further assess how ECM remodeling differs between OA and non-OA chondrocytes, we analyzed matrix degradation activity by embedding chondrocytes in a 3D PEG hydrogel mixed with a Alexa 488 dye labeled gelatin to get a uniformly fluorescent hydrogel. Quantification of the degraded area revealed that OA cells demonstrate higher matrix degradation (Fig. 3k, 3m) which may facilitate cellular volume expansion in response to a compromised ECM. Additionally, we observed that degradation occurred primarily around the cell body rather than

at protrusions in both groups, with similar spatial patterns observed in both OA and non-OA cells (Fig. 3n). This suggests that while OA chondrocytes exhibit distinct alterations in adhesion and actin organization, their overall matrix-degrading activity around protrusions in 3D does not differ significantly from non-OA cells.

Together, these findings illustrate that, in a 3D degradable PEG-RGD hydrogel environment, OA chondrocytes exhibit distinct morphological and cytoskeletal alterations—namely, increased cell volume, enhanced actin polymerization, more extensive protrusive activity, and decreased β1 integrin and fibronectin levels, compared to non-OA cells.

OA cells show more contractile phenotype than healthy cells.

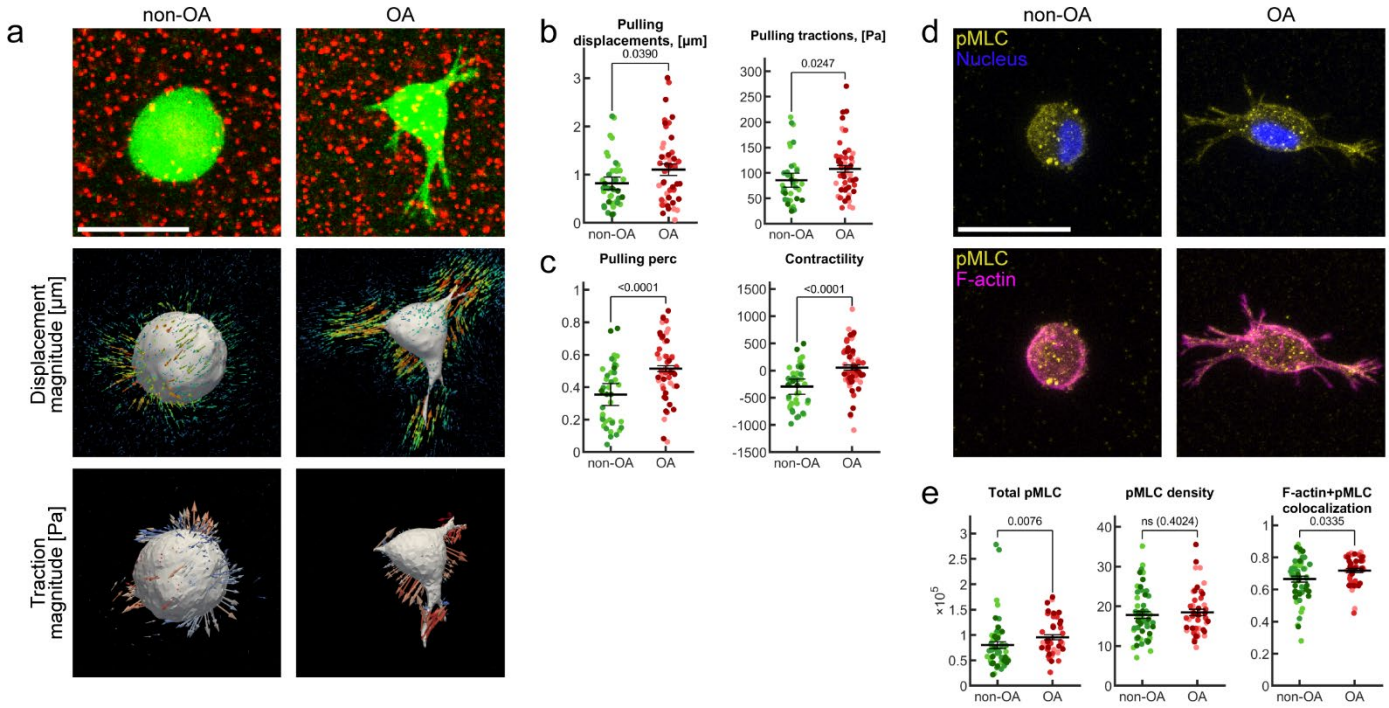

Figure 4. ***a*** *3D TFM results illustration. (top) Representative maximum projected images of beads (red) and chondrocyte (green) for one non-OA and one OA chondrocyte. (middle) Corresponding 3D displacement magnitude renders. (bottom) Corresponding 3D traction force magnitude renders.* ***b*** *Quantification of the 99th percentile pulling (inward oriented) bead displacement magnitude [µm] and pulling (inward oriented) traction force magnitude [Pa].* ***c*** *Quantification of the percentage of pulling traction force vectors per cell. Quantification of contractility, sum of all traction force vectors projected on the axis connecting the corresponding node to the cell centroid.* ***d*** *Maximum intensity projection of pMLC (yellow) and overlay with F-actin (magenta) for a representative non-OA and OA chondrocyte.* ***e*** *Quantification of pMLC expression: total pMLC intensity of a cell, total pMLC intensity normalized by the cell area, pMLC intensity in the cell cortex normalized by total pMLC intensity, Colocalization of F-actin with pMLC. All statistical comparisons used generalized linear mixed-effects models to account for the nested structure of the data. Error bars represent SEM, scalebars are 30 µm. Each green and red hue in the graph represents a different patient (N=3 for each condition), each dot represents the value for one cell (n≥15 for every patient).*

Building upon the more protrusive phenotype of OA chondrocytes characterized by increased actin intensity and protrusions, we wondered if OA chondrocytes possess an improved force generation capacity. Traction forces serve as direct indicators of a cell's ability to generate mechanical work on its surrounding matrix, which contributes to matrix remodeling, signaling etc. To further investigate the mechanobiological behavior of chondrocytes in a three-dimensional context, we performed 3D TFM experiments using the same degradable PEG hydrogel system functionalized with RGD peptides embedded with 200nm fluorescent beads. Cells were encapsulated in the gel and imaged 24 hours after seeding (Fig. 4a).

Quantitative analysis of the 3D TFM data revealed both pulling (inward oriented) and pushing (outward oriented) traction forces. OA chondrocytes exhibited a more pulling phenotype compared to non-OA chondrocytes, evidenced by a higher percentage of pulling traction forces (Fig. 4c). Interestingly, OA chondrocytes favor a contractile phenotype, evidenced by higher pulling displacements and traction forces compared to non-OA chondrocytes (Fig. 4b). Moreover, when looking at contractility as a global metric of the cell's ability to generate contractile forces, OA chondrocytes showed an increased contractility (Fig. 4c), reflecting a more contractile OA cell phenotype when put in soft 3D degradable environment

When analyzing the pushing traction forces, we could link the inward displacements to cell volume decrease between the stressed and relaxed state (Fig. S3a). This shows that the pushing forces observed are due to a volume decrease effect of Cyto D relaxation. Moreover, we didn't observe a difference in pushing displacements and pushing traction forces (Fig. S3b), indicating that the volume decrease is an effect independent of pathological condition.

Since we observed a more contractile phenotype for OA chondrocytes, we asked how this was related to pMLC levels. In agreement with our previous 2D observations, immunostaining for pMLC further demonstrated that OA cells possess a higher total amount of pMLC and similar pMLC density between OA and non-OA cells (Fig. 4d, 4e), suggesting that the increased pMLC content is proportional to the enlarged cell size in OA. Combining increased pMLC content and increased actin cytoskeleton, we suspect an elevated actomyosin coupling. Additionally, we observed increased colocalization of F-actin with pMLC in OA chondrocytes. These findings combined could be the driver of enhance contractility.

This enhanced coupling likely reinforces force generation and transmission despite alterations in cell morphology and adhesion, shown as decreased β1 integrin and fibronectin levels for OA cells in our previous experiments. This reinforcement allows for a cell to create contractile forces, opposite to what we observed in a 2D case, offering insights into how OA chondrocytes adapt their mechanobiological responses in a physiologically relevant 3D degradable matrix environment in comparison to a 2D substrate.

These findings suggest that in a 3D degradable matrix, OA chondrocytes not only generate greater forces but also exhibit a more tightly coupled actomyosin network. The elevated pulling displacements and traction forces indicate that OA cells adapt to the degradable, dynamic environment by upregulating contractile mechanisms, possibly as a compensatory response to altered cell–ECM interactions. Furthermore, the increased colocalization of F-actin and pMLC points to a more coordinated assembly of contractile machinery, which may enhance force transmission and mechanosensing. Together, these results underscore the complex interplay between cytoskeletal organization and contractile function in OA chondrocytes, highlighting potential mechanisms by which altered cell mechanics contribute to disease progression.

Moreover, the interplay between cellular mechanobiology and inflammatory signaling pathways in OA chondrocytes requires further investigation. The altered mechanical environment resulting from ECM degradation may not only affect cytoskeletal organization but could also exacerbate inflammatory responses through enhanced cytokine production. For instance, it has been shown that pro-inflammatory cytokines such as IL-1β can significantly modulate actin dynamics and integrin expression, potentially leading to a vicious cycle of inflammation and tissue degeneration [1]. This relationship underscores the need for therapeutic strategies that target both the biomechanical aspects and the inflammatory environment in OA, aiming to restore normal cellular function while mitigating the pathological feedback loops initiated by chronic inflammation. Addressing these interconnected pathways

could pave the way for more effective interventions aimed at halting or reversing the progression of osteoarthritis.

Discussion

Our study provides insights into the mechanobiological changes in osteoarthritic chondrocytes compared to healthy cells, revealing notable differences in cell morphology, cytoskeletal organization, integrin distribution, and extracellular matrix interactions.

The hypertrophic enlargement of OA chondrocytes observed on both 2D and 3D substrates is consistent with prior reports linking increased cell size in OA to aberrant differentiation and an inflammatory microenvironment [6], [22]. This enlargement, accompanied by reduced F-actin density in 2D, indicates a decoupling of cell expansion from cytoskeletal support, leading to cytoskeletal dysregulation rather than increased contractility. This may represent a compensatory mechanism of OA chondrocytes striving to maintain function despite structural deficiencies [21].

The observed reorganization of the cytoskeleton in OA chondrocytes in 2D, marked by a more uniform F-actin distribution, may reflect altered mechanotransduction pathways. Disruption in actin organization could impair the chondrocyte's ability to sense mechanical stimuli, thereby contributing to OA progression [23]. This relationship between cytoskeletal integrity and mechanotransduction is further supported by evidence that cytoskeletal disruptions can lead to altered gene expression profiles in OA chondrocytes [24]. Moreover, ECM stiffness has been shown to significantly affect chondrocyte behavior and gene expression, potentially influencing OA progression [21]. Recent findings also suggest that mechanosensitive ion channels in chondrocytes play a critical role in mediating the effects of mechanical forces on chondrocyte homeostasis, further linking mechanotransduction to OA pathology [27].

The reduced density of β1 integrin in OA chondrocytes, despite unchanged total expression levels, suggests impaired integrin localization and functional clustering. This aligns with the understanding that integrin dysfunction is a hallmark of OA progression, as integrins are essential for mediating cell-ECM interactions and signaling [5], [25]. Decreased focal adhesion formation in OA cells may compromise their ability to respond to mechanical cues, potentially exacerbating the catabolic environment characteristic of OA. Studies have emphasized that integrin signaling pathways are crucial for maintaining chondrocyte homeostasis, and their disruption can lead to increased catabolic activity and cartilage degradation [28].

In summary, our study underscores the various mechanobiological alterations in OA chondrocytes, including changes in cell morphology, cytoskeletal organization, integrin function, and ECM composition. These insights not only deepen our understanding of OA pathogenesis but also highlight potential targets for therapeutic intervention aimed at restoring normal chondrocyte function and preventing disease progression.

Methods

Cell culture

Healthy and osteoarthritic primary cells were isolated from explants of patients that underwent hip replacement surgery in the university hospital Gasthuisberg, KULeuven. Non-OA primary cells were collected from three patients that had surgery for osteoporotic or malignancy associated fractures with no history of OA (two-woman, one man, age 44, 77 and 90). OA primary cells were obtained from three OA patients undergoing hip surgery (one woman, two men, age 64, 71 and 82). Primary human articular chondrocytes (hACs) were isolated as previously described [29]. Briefly, cartilage was first dissected from the joint surface, rinsed with phosphate buffered saline (PBS), and cut into small pieces. The cartilage pieces were incubated with 2 mg/ml pronase solution (Roche) for 90 minutes at 37°C and digested overnight at 37°C in 1.5 mg/ml collagenase B solution (Roche). Then, the preparation was filtered through a 70 µM strainer and cells were plated in culture flasks (T75, Avantor) and cultured in a humidified atmosphere at 37°C and 5% CO2. Culture medium consisted of Dulbecco's Modified Eagle Medium F12 (DMEM/F12, Gibco), 10% fetal bovine serum (FBS, Gibco), 1% (vol/vol antibiotic/antimycotic (Gibco), and 1% L-glutamine (Gibco). All cells were used between P0 and P2.

PAA hydrogel preparation

Polyacrylamide hydrogels of 4.5kPa were prepared according to previously reported protocols. Fluorescent beads (Invitrogen, FluoSpheres Carboxylate-Modified Microspheres, 200 nm) were added to the hydrogel mixture (1:60 concentration) for TFM samples. Briefly, MilliQ, sonicated fluorescent beads , 40% Acrylamide (Sigma-Aldrich, A4058) and 2% bisacrylamide (Sigma-Aldrich, M1533) were mixed in that order. Hydrogel polymerization was initialized by ammonium persulfate (4.4 µM) and catalysed by N,N,N',N'-tetramethylethylenediamine (Sigma-Aldrich, T7024). A 15 µl hydrogel droplet was placed on the bottom of a 6 well plate with glass bottom (Cellvis, P06-14-0-N), pre-treated with bind-silane (Serva, 28739.01). The hydrogel was flattened with a coverslip glass, pre-treated with Sigmacote and left to polymerize at room temperature for 30 minutes. The gel surface is functionalized by two rounds of 0.67 µM Sulfo-SANPAH (Sigma-Aldrich, 803332) treatment under UV-irradiation with 365 nm wavelength emission for 30 minutes, followed by a 2 hour incubation at 37 °C in 10 µg/ml Fibronectin (human plasma, Sigma-Aldrich) diluted in 0.1% v/v acetic acid at pH 3.4 for homogeneous coating [30]. 3000 cells were seeded per hydrogel and allowed to spread for 24 hours. Afterwards, samples were either live imaged for TFM experiments or fixed for half an hour in 4% paraformaldehyde for immunostaining. PAA hydrogels were characterized as previously described in [31].

PEG hydrogel preparation

Degradable polyethylene glycol (PEG) precursors and buffers were prepared as previously described [32]. Fluorescent beads (Invitrogen , FluoSpheres Carboxylate-Modified Microspheres, 200 nm) were added to the hydrogel mixture (1:60 v/v concentration) for TFM samples. Briefly, milliQ water, sonicated fluorescent beads, 10X Buffer, lysine-RGD (50 µM, Pepmic), PEG and cell solution were mixed in that order. The cell concentration was calculated to have 3000 chondrocytes per hydrogel droplet. Enzymatic crosslinking was initialized by addition of activated FXIII. We used a w/v hydrogel composition of 1.2% at Youngs modulus of 520 Pa. A 18 µl hydrogel droplet was placed on the bottom of an Imaging chamber (µ-Slide 18 Well, Ibidi) and allowed to crosslink at 37 °C and 5% CO2 for 30 minutes. Afterwards culture medium was added, and cells were incubated for 24 hours. Afterwards, samples were either

live imaged for TFM experiments or fixed for half an hour in 4% paraformaldehyde for immunostaining and matrix degradation quantification. PEG hydrogels were characterized as previously described in [32].

2D Immunofluorescence staining

Hydrogels for immunofluorescence were fixed for half an hour in 4% paraformaldehyde followed by washing with PBS.

Immunostaining of pMLC requires permeabilization of the cell membrane with Permeabilization solution constituting 0.3% Triton X (10%) in PBS 1X at room temperature for 1 hour. Subsequently, samples were treated with permeabilizing blocking solution constituting 1% BSA, 10% goal serum and 1% Triton X (10%) at room temperature for four hours and half. Primary antibody Phospho-Myosin Light Chain 2 (Ser19) (Cell Signaling Technology #3671 1:100) was suspended in permeabilizing blocking solution and applied to the sample and incubated at 37°C and 5% CO2 for 1 hour and half. The sample was washed with Rinsing solution constituting 0.05% TWEEN 20 in PBS 1X and incubated at 4°C on a shaker overnight. The following day, three washes with rinsing solution were carried out every two hours. Goat anti-Rabbit IgG secondary antibody conjugated with Alexa Fluor 488 (Invitrogen, 1:1000) was diluted in permeabilizing blocking solution and incubated at 37°C and 5% CO2 for 1 hour and half. Afterwards, the sample was washed with Rinsing solution and put overnight on a shaker at 4°C. The following day, three washes with rinsing solution were carried out every two hours.

For immunostaining of β1 integrin and fibronectin, the following protocol was followed. First, samples were treated with non-permeabilizing blocking solution constituting 1% BSA, 10% goal serum and 0.05% Tween 20 for four hours and half. Primary antibodies were suspended in non-permeabilizing blocking solution and applied to the sample and incubated at 37°C and 5% CO2 for 1 hour and half. Anti-fibronectin antibody (Sigma-Aldrich, F3648 1:1000) and anti-β1 Integrin antibody (BD Biosciences #553715, 1:200) were used as primary antibodies. The following day, three washes with rinsing solution were carried out every two hours and the sample was kept at 4°C on a shaker in between washes. Goat anti-Rabbit IgG secondary antibody conjugated with Alexa Fluor 488 (Invitrogen, 1:1000) and Goat anti-Rat IgG secondary antibody conjugated with Alexa Fluor 546 (Invitrogen, 1:1000) were diluted in non-permeabilizing blocking solution and incubated at 37°C and 5% CO2 for 1 hour and half. Afterwards, the sample was washed with Rinsing solution and incubated at 4°C on a shaker overnight. The following day, three washes with rinsing solution were carried out every two hours and the sample was kept at 4°C on a shaker in between washes.

Then, for all 2D samples, phalloidin conjugates with Atto 647 (Sigma-Aldrich, 1:2000) were diluted in PBS and applied to the sample, incubating on a shaker at 4°C for 45 minutes. Finally, DAPI (1:5000) diluted in PBS was applied to the sample and incubated for ten minutes at room temperature. Samples were extensively washed with rinsing solution before imaging.

3D Immunofluorescence staining

Hydrogels for immunofluorescence were fixed for half an hour in 4% paraformaldehyde followed by washing with PBS.

Immunostaining of pMLC requires permeabilization of the cell membrane with Permeabilization solution constituting 0.3% Triton X (10%) in PBS 1X at 37°C and 5% CO2 for half an hour. Subsequently, samples were treated with permeabilizing blocking solution constituting 1% BSA, 10% goal serum and 1% Triton X (10%) at room temperature for four hours and half. Primary antibody Phospho-Myosin Light Chain 2 (Ser19) (Cell Signaling Technology #3671 1:50) was suspended in permeabilizing blocking solution and applied to the

sample and incubated at 4°C on a shaker overnight. The following day, five washes with rinsing solution were carried out every two hours and the sample was kept at 4°C on a shaker in between washes. Then, Goat anti-Rabbit IgG secondary antibody conjugated with Alexa Fluor 488 (Invitrogen, 1:500) was diluted in permeabilizing blocking solution and incubated at 4°C on a shaker overnight. The following day, five washes with rinsing solution were carried out every two hours and the sample was kept at 4°C on a shaker in between washes.

For immunostaining of β1 integrin and fibronectin, the following protocol was followed. First, samples were treated with non-permeabilizing blocking solution constituting 1% BSA, 10% goal serum and 0.05% Tween 20 for four hours and half. Primary antibodies were suspended in non-permeabilizing blocking solution and applied to the sample and incubated at 4°C on a shaker overnight. Anti-fibronectin antibody (Sigma-Aldrich, F3648 1:500) and anti-β1 Integrin antibody (BD Biosciences #553715, 1:100) were used as primary antibodies. The following day, five washes with rinsing solution were carried out every two hours and the sample was kept at 4°C on a shaker in between washes. Goat anti-Rabbit IgG secondary antibody conjugated with Alexa Fluor 488 (Invitrogen, 1:500) and Goat anti-Rat IgG secondary antibody conjugated with Alexa Fluor 546 (Invitrogen, 1:500) were diluted in non-permeabilizing blocking solution and incubated at 4°C on a shaker overnight. The following day, five washes with rinsing solution were carried out every two hours and the sample was kept at 4°C on a shaker in between washes. Then, for all 3D samples, phalloidin conjugates with Atto 647 (Sigma-Aldrich, 1:1000) were diluted in PBS and applied to the sample, incubating on a shaker at 4°C for four hours. Finally, DAPI (1:2000) diluted in PBS was applied to the sample and incubated for ten minutes at room temperature. Samples were extensively washed with rinsing solution before imaging.

Traction force microscopy image acquisition

All live cell imaging for TFM was done using a Leica TCS SP8 confocal fluorescence microscope. For TFM, confocal images were acquired using a 40X water objective using 1.5 zoom at a 512x512 resolution at 1AU and bidirectional imaging with phase correction. Excitation wavelengths were set to 488 nm (green cell channel) and 563 nm (red beads channel). The detection wavelengths of the hybrid detectors were set to 495-555 nm and 570-630 nm respectively to minimize crosstalk between the green and red channel and allow for simultaneous imaging. Stressed state images were collected as z-stacks with 0.5 μm step size.

For 2D samples, relaxed state was induced by removing the cells by addition of a droplet of 5% Sodium dodecyl sulphate (SDS). After 15 minutes, the hydrogel returned to a stress-free state and relaxed state bead images were acquired using the same imaging settings.

For 3D samples, relaxed state was induced by depolymerizing actin by addition of Cytochalasin D (dissolved in DMSO, Sigma Aldric) at a final concentration of 4 μM. After 1 hour, the hydrogel returned to a stress-free state and relaxed state bead images were acquired using the same imaging settings.

2D traction force microscopy analysis

2D TFM analysis was performed using a previously described computational framework implemented in MATLAB [31]. Briefly, beads and cell images were filtered using a Gaussian kernel to suppress noise. Cell masks, used to calculate the metrics in Fig. 2b, were obtained by thresholding the cell channel. Unwanted spatial shifts between the stressed and relaxed state image stacks were corrected for by rigid image registration using the findshift function from the DipImage library [33]. Cell-induced displacements in the bead images were measured using a non-rigid, free-form deformation image registration method [34] using the Elastix

toolbox [35]. Tractions were recovered by considering PAA gels as homogeneous, isotropic, linear elastic half spaces and applying a modified Tikhonov regularized Fourier transform traction cytometry algorithm [36]. Since noise levels in the measured displacement fields were similar throughout the dataset, a constant value of 10 was set for the Tikhonov regularization parameter lambda. Maximum displacements, maximum tractions, contractility and cortical force metrices were restricted to the area of the cell mask.

3D traction force microscopy analysis

3D TFM images were analyzed using the TFMLAB software toolbox [37] and as described in [32]. The hydrogel was modeled as a linear elastic material with Youngs Modulus E=520 Pa and Poisson ration $\nu = 0.3$. To analyse the TFM data, different metrices were defined. The activeness of a cell is determined by the percentage of displacements in the vicinity of the cell that are larger than the pixel size (0.38 µm). A cell is deemed passive when this percentage is below 1 %. To determine whether a traction force is pulling or pushing, the traction force magnitude vector at a node was projected onto the vector that connects the node with the centre of the cell. Then, based on the sign of the projected traction force, it can be categorized as pulling (positive sign) or pushing (negative sign). The maximum pulling and pushing traction force are computed using this categorization. The pulling percentage displayed in Fig. 4c is the percentage of positive traction force projections per cell. The contractility of each cell is defined by summing all the projected traction forces.

Immunofluorescence image acquisition

All immunofluorescence imaging was done using a Leica TCS SP8 confocal fluorescence microscope. Confocal images were acquired using a 25X water objective using 3.4 zoom at a 512x512 resolution at 1AU. Excitation wavelengths were set to 405 nm (Blue nucleus channel), 488 (Green pMLC or Fibronectin channel), 563 nm (Red β1 integrin channel) and 647 (Far red Phalloidin channel). The emission wavelengths of the Hybrid detectors were 410-460 nm, 495-555 nm, 570-630 nm and 666-753 nm respectively. To avoid crosstalk between the channels, they were imaged sequentially: sequence 1 - Blue and Far red channel, sequence 2 - Green channel and sequence 3 - Red channel. 3D image z-stacks were acquired with a 0.5 µm step size.

For imaging of the degradation assay, a Leica TCS SP8 confocal fluorescence microscope was used. Confocal images were acquired using a 25X water objective using 3.4 zoom at a 512x512 resolution at 1AU and bidirectional imaging with phase correction. Excitation wavelengths were set to 405 nm (Blue nucleus channel), 488 nm (Green gelatin channel) and 647 nm (Far red Phalloidin channel). The emission wavelengths of the Hybrid detectors were set to were 410-460 nm, 495-555 nm and 670-730 nm respectively. To avoid crosstalk between the channels, they were imaged sequentially: sequence 1 - Blue and Far red channel and sequence 2 – Green channel. 3D image z-stacks were acquired with a 0.5 µm step size.

Quantification of cell morphology and actin

3D fluorescence image stacks of 2D and 3D samples are maximally projected and filtered with a median filter. Cell segmentation of the cells was done using a manually adjusted intensity threshold. Area, Solidity. Eccentricity and Circularity were computed using the regionprops function in MATLAB (Fig. S4). Protrusions were segmented as described in [32] (Fig. S6). Briefly, an opening operation on the cell segmentation using a disk-shaped structuring element of a 7 pixels radius. The number of the protrusions was counted and using *regionprops*, the protrusion area and max protrusion length was calculated. Total actin intensity metric was obtained by summing the actin intensity values within the cell segmentation. The actin density

was obtained by normalizing the total actin intensity by the area. To measure the amount of actin in the cell cortex, a cortex mask was created (Fig. S5). Briefly, the cell segmentation was skeletonized to get the cell boundary and dilated inside with a disk-shaped structuring element of 20 pixels. The cortical metrices shown in Fig. 1 are calculated by taking the ratio the sum of actin intensities within the cortex over the total actin intensity.

Quantification of nucleus morphology

3D fluorescence DAPI image stacks of 2D and 3D samples are maximally projected and filtered with a median filter. Cell segmentation of the nuclei was done using automated Otsu thresholding. Area, Solidity. Eccentricity and Circularity were computed using the regionprops function in MATLAB.

Quantification of pMLC and Fibronectin

3D fluorescence image stacks of 2D and 3D samples are maximally projected. Cell segmentation of the cells was done using a manually adjusted intensity threshold. Total pMLC intensity was computed by summing the pMLC intensity within the cell segmentation. pMLC density was computed by normalizing the total pMLC intensity by the cell area. Total fibronectin was computed by summing the fibronectin intensity within a dilated cell mask (using a disk-shaped structure element with radius 5). The fibronectin density is computed by taking the mean of the fibronectin intensity within the dilated cell area.

Colocalization of two metrics (actin-fibronectin and actin-pMLC) within a cell is reported as the correlation coefficient and is computed using the projected fluorescent z-stacks and the corr2 function in MATLAB. Prior to the computation, the respective fluorescent images are blurred using a Gaussian smoothing kernel with standard deviation of 0.5 (function *imgaussfilt* in MATLAB).

Quantification of β1 integrin

For the β1 integrin immunostaining, we were only interested in the β1 integrin located at the cell membrane, since this is where forces are transduced to the ECM.

For 2D samples, the hydrogel-cell interface was located using the following steps: a rudimentary 3D cell segmentation of the phalloidin was obtained using Otsu thresholding. The centroid of the cell was determined using the function regionprops. Based on this centroid, a maximum projection was made of only the bottom z-slices of the 3D fluorescence β1 integrin image stacks. This maximum projection is further used for the quantifications. The total β1 integrin intensity is computed by summing the β1 integrin intensity within the cell segmentation. The β1 integrin density is computed by taking the mean of the β1 integrin intensity withing the cell segmentation.

3D fluorescence β1 integrin image stacks of 3D samples are maximally projected. Cell and cortex segmentation of the cells was done using a manually adjusted intensity threshold. The total β1 integrin intensity is computed by summing β1 integrin intensity within the cell cortex. The β1 integrin density is computed by taking the mean of the β1 integrin intensity withing the cell cortex. Colocalization of two metrics (actin-β1 integrin and fibronectin-β1 integrin) within a cell is reported as the correlation coefficient and is computed as explained above using the projected fluorescent z-stacks.

Quantification of matrix degradation

Gelatin labeled with Alexa 488 dye (1:20 concentration) was added to the PEG hydrogel solution to give a uniformly fluorescent hydrogel. The matrix degraded area was quantified as

described in [32]. An additional image processing workflow was used to distinguish the degradation around the cell body and the protrusions (Fig. S7).

A cell segmentation of the cell is created using Otsu thresholding. Subsequently, the cell segmentation is divided into two masks: the cell body and the protrusions, by applying an opening operation on the cell segmentation using a disk-shaped structuring element of a 20 pixels radius. The cell body mask and protrusion mask are dilated by one pixel for thirty steps and a mean gelatin intensity within the dilated mask is computed for each step. The degradation around the cell body and protrusions visualized in Fig. 3n are computed using this workflow.

Statistics

Statistical analysis was performed using generalized linear mixed-effects models (GLMMs) to account for the nested structure of the data (cells within patients from two conditions) and to test for differences between experimental conditions [20, F. Tuerlinckx *et al.*, 2006, DOI.]. The choice of distribution and link function was tailored to the properties of each metric. For data that passed the Shapiro-Wilk normality test, a normal distribution was used. Non-normal, positive, unbounded data were modeled using a gamma distribution with a log link, while count data were analyzed using a Poisson distribution with a log link. For metrics bounded between 0 and 1, a logit transformation was applied, and the transformed data were modeled using a normal distribution. Model diagnostics were performed to ensure numerical stability and appropriate fit. Statistical significance was assessed using the Wald test. All analyses were conducted using MATLAB (version R2024b, MathWorks). This approach allows for robust statistical inference while accounting for the complex structure of the experimental data, as recommended by [21, B. M. Bolker *et al.*, 2009, DOI.] and [22, S. Nakagawa and H. Schielzeth, 2010, DOI.]

Acknowledgements

The authors acknowledge financial support from KU Leuven grant IDN/20/019.

References

[1] S. R. Goldring and M. B. Goldring, “The Role of Cytokines in Cartilage Matrix Degeneration in Osteoarthritis,” *Clinical Orthopaedics and Related Research®*, vol. 427, p. S27, Oct. 2004, doi: 10.1097/01.blo.0000144854.66565.8f.

[2] N. A. Al-Maslamani *et al.*, “Chondrocyte De-Differentiation: Biophysical Cues to Nuclear Alterations,” *Cells*, vol. 11, no. 24, p. 4011, Dec. 2022, doi: 10.3390/cells11244011.

[3] K. Kong *et al.*, “Mechanical overloading leads to chondrocyte degeneration and senescence via Zmpste24-mediated nuclear membrane instability,” *iScience*, vol. 26, no. 11, p. 108119, Oct. 2023, doi: 10.1016/j.isci.2023.108119.

[4] Z. Zhao, Y. Li, M. Wang, S. Zhao, Z. Zhao, and J. Fang, “Mechanotransduction pathways in the regulation of cartilage chondrocyte homoeostasis,” *J Cell Mol Med*, vol. 24, no. 10, pp. 5408–5419, May 2020, doi: 10.1111/jcmm.15204.

[5] R. F. Loeser, “Integrins and chondrocyte-matrix interactions in articular cartilage,” *Matrix Biol*, vol. 39, pp. 11–16, Oct. 2014, doi: 10.1016/j.matbio.2014.08.007.

[6] J. C. Lauer, M. Selig, M. L. Hart, B. Kurz, and B. Rolauffs, “Articular Chondrocyte Phenotype Regulation through the Cytoskeleton and the Signaling Processes That Originate from or Converge on the Cytoskeleton: Towards a Novel Understanding of the Intersection between Actin Dynamics and Chondrogenic Function,” *Int J Mol Sci*, vol. 22, no. 6, p. 3279, Mar. 2021, doi: 10.3390/ijms22063279.

[7] W. Dessau, J. Sasse, R. Timpl, F. Jilek, and K. von der Mark, “Synthesis and extracellular deposition of fibronectin in chondrocyte cultures. Response to the removal of extracellular cartilage matrix.,” *Journal of Cell Biology*, vol. 79, no. 2, pp. 342–355, Nov. 1978, doi: 10.1083/jcb.79.2.342.

[8] G. A. Homandberg, C. Wen, and F. Hui, “Cartilage damaging activities of fibronectin fragments derived from cartilage and synovial fluid,” *Osteoarthritis Cartilage*, vol. 6, no. 4, pp. 231–244, Jul. 1998, doi: 10.1053/joca.1998.0116.

[9] J. Song, X. Zeng, C. Li, H. Yin, S. Mao, and D. Ren, “Alteration in cartilage matrix stiffness as an indicator and modulator of osteoarthritis,” *Biosci Rep*, vol. 44, no. 1, p. BSR20231730, Jan. 2024, doi: 10.1042/BSR20231730.

[10] M. M. J. Caron *et al.*, “Redifferentiation of dedifferentiated human articular chondrocytes: comparison of 2D and 3D cultures,” *Osteoarthritis and Cartilage*, vol. 20, no. 10, pp. 1170–1178, Oct. 2012, doi: 10.1016/j.joca.2012.06.016.

[11] Q. Zhang, Y. Yu, and H. Zhao, “The effect of matrix stiffness on biomechanical properties of chondrocytes,” *Acta Biochimica et Biophysica Sinica*, vol. 48, no. 10, pp. 958–965, Oct. 2016, doi: 10.1093/abbs/gmw087.

[12] K. S. Rankin, R. L. Lakey, C. H. Gerrand, A. P. Sprowson, A. W. McCASKIE, and M. A. Birch, “A Novel in Vitro Model to Investigate Behavior of Articular Chondrocytes in Osteoarthritis,” *The Journal of Rheumatology*, vol. 37, no. 2, pp. 426–431, Feb. 2010, doi: 10.3899/jrheum.080080.

[13] N. L. Bergholt *et al.*, “Surface chemistry, substrate, and topography guide the behavior of human articular chondrocytes cultured in vitro,” *Journal of Biomedical Materials Research Part A*, vol. 106, no. 11, pp. 2805–2816, 2018, doi: 10.1002/jbm.a.36467.

[14] E. Schuh, S. Hofmann, K. S. Stok, H. Notbohm, R. Müller, and N. Rotter, “The influence of matrix elasticity on chondrocyte behavior in 3D,” *Journal of Tissue Engineering and Regenerative Medicine*, vol. 6, no. 10, pp. e31–e42, 2012, doi: 10.1002/term.501.

[15] P. Yeung, K. H. Cheng, C. H. Yan, and B. P. Chan, “Collagen microsphere based 3D culture system for human osteoarthritis chondrocytes (hOACs),” *Scientific Reports*, vol. 9, no. 1, Aug. 2019, doi: 10.1038/s41598-019-47946-3.

[16] H. Li *et al.*, “Evaluating Osteoarthritic Chondrocytes through a Novel 3-Dimensional In Vitro System for Cartilage Tissue Engineering and Regeneration,” *CARTILAGE*, vol. 3, no. 2, pp. 128–140, Feb. 2012, doi: 10.1177/1947603511429698.

[17] K. M. Pichler *et al.*, “The Dysregulated Galectin Network Activates NF-κB to Induce Disease Markers and Matrix Degeneration in 3D Pellet Cultures of Osteoarthritic Chondrocytes,” *Calcified Tissue International*, vol. 108, no. 3, pp. 377–390, Nov. 2020, doi: 10.1007/s00223-020-00774-4.

[18] C. Chen, J. Xie, L. Deng, and L. Yang, “Substrate Stiffness Together with Soluble Factors Affects Chondrocyte Mechanoresponses,” *ACS Appl. Mater. Interfaces*, vol. 6, no. 18, pp. 16106–16116, Sep. 2014, doi: 10.1021/am504135b.

[19] C. Chen *et al.*, “Effects of vimentin disruption on the mechanoresponses of articular chondrocyte,” *Biochemical and Biophysical Research Communications*, vol. 469, no. 1, pp. 132–137, Jan. 2016, doi: 10.1016/j.bbrc.2015.11.083.

[20] G. Zhen *et al.*, “Mechanical stress determines the configuration of TGFβ activation in articular cartilage,” *Nat Commun*, vol. 12, no. 1, p. 1706, Mar. 2021, doi: 10.1038/s41467-021-21948-0.

[21] J.-H. Kim *et al.*, “Matrix cross-linking–mediated mechanotransduction promotes posttraumatic osteoarthritis,” *Proceedings of the National Academy of Sciences*, vol. 112, no. 30, pp. 9424–9429, Jul. 2015, doi: 10.1073/pnas.1505700112.

[22] P. Gratal *et al.*, “Chondrocyte enlargement is a marker of osteoarthritis severity,” *Osteoarthritis and Cartilage*, vol. 27, no. 8, pp. 1229–1234, Aug. 2019, doi: 10.1016/j.joca.2019.04.013.

[23] F. Guilak, “Compression-induced changes in the shape and volume of the chondrocyte nucleus,” *J Biomech*, vol. 28, no. 12, pp. 1529–1541, Dec. 1995, doi: 10.1016/0021-9290(95)00100-x.

[24] N. Pascarelli, G. Collodel, E. Moretti, S. Cheleschi, and A. Fioravanti, “Changes in Ultrastructure and Cytoskeletal Aspects of Human Normal and Osteoarthritic Chondrocytes Exposed to Interleukin-1β and Cyclical Hydrostatic Pressure,” *IJMS*, vol. 16, no. 11, pp. 26019–26034, Oct. 2015, doi: 10.3390/ijms161125936.
[25] R. F. Loeser, C. S. Carlson, and M. P. McGee, “Expression of β1 Integrins by Cultured Articular Chondrocytes and in Osteoarthritic Cartilage,” *Experimental Cell Research*, vol. 217, no. 2, pp. 248–257, Apr. 1995, doi: 10.1006/excr.1995.1084.
[26] T. Yasuda, “Cartilage destruction by matrix degradation products,” *Mod Rheumatol*, vol. 16, no. 4, pp. 197–205, Jan. 2006, doi: 10.1007/s10165-006-0490-6.
[27] K. Zhang *et al.*, “Mechanosensory and mechanotransductive processes mediated by ion channels in articular chondrocytes: Potential therapeutic targets for osteoarthritis,” *Channels*, vol. 15, no. 1, pp. 339–359, Jan. 2021, doi: 10.1080/19336950.2021.1903184.
[28] H. Jin, S. Jiang, R. Wang, Y. Zhang, J. Dong, and Y. Li, “Mechanistic Insight Into the Roles of Integrins in Osteoarthritis,” *Front. Cell Dev. Biol.*, vol. 9, Jun. 2021, doi: 10.3389/fcell.2021.693484.
[29] R. Castro-Viñuelas, N. Viudes-Sarrión, A. V. Rojo-García, S. Monteagudo, R. J. Lories, and I. Jonkers, “Mechanical loading rescues mechanoresponsiveness in a human osteoarthritis explant model despite Wnt activation,” *Osteoarthritis and Cartilage*, Mar. 2024, doi: 10.1016/j.joca.2024.02.945.
[30] A. E. Stanton, X. Tong, and F. Yang, “Varying solvent type modulates collagen coating and stem cell mechanotransduction on hydrogel substrates,” *APL Bioengineering*, vol. 3, no. 3, p. 036108, Sep. 2019, doi: 10.1063/1.5111762.
[31] S. Aytekin *et al.*, “Linking Molecular Tension and Cellular Tractions: A Multiscale Approach to Focal Adhesion Mechanics,” Jan. 13, 2025, *bioRxiv*. doi: 10.1101/2025.01.09.632081.
[32] A. Shapeti *et al.*, “Force-mediated recruitment and reprogramming of healthy endothelial cells drive vascular lesion growth,” *Nat Commun*, vol. 15, no. 1, p. 8660, Oct. 2024, doi: 10.1038/s41467-024-52866-6.
[33] “DIPimage.” Accessed: Feb. 26, 2025. [Online]. Available: https://diplib.org/DIPimage.html
[34] A. Jorge-Peñas *et al.*, “Free Form Deformation–Based Image Registration Improves Accuracy of Traction Force Microscopy,” *PLOS ONE*, vol. 10, no. 12, p. e0144184, Dec. 2015, doi: 10.1371/journal.pone.0144184.
[35] S. Klein, M. Staring, K. Murphy, M. A. Viergever, and J. P. W. Pluim, “elastix: A Toolbox for Intensity-Based Medical Image Registration,” *IEEE Transactions on Medical Imaging*, vol. 29, no. 1, pp. 196–205, Jan. 2010, doi: 10.1109/TMI.2009.2035616.
[36] A. Izquierdo-Álvarez, D. A. Vargas, Á. Jorge-Peñas, R. Subramani, M.-M. Vaeyens, and H. Van Oosterwyck, “Spatiotemporal Analyses of Cellular Tractions Describe Subcellular Effect of Substrate Stiffness and Coating,” *Ann Biomed Eng*, vol. 47, no. 2, pp. 624–637, Feb. 2019, doi: 10.1007/s10439-018-02164-2.
[37] J. Barrasa-Fano, A. Shapeti, Á. Jorge-Peñas, M. Barzegari, J. A. Sanz-Herrera, and H. V. Oosterwyck, “TFMLAB: A MATLAB toolbox for 4D traction force microscopy,” *SoftwareX*, vol. 15, Jul. 2021, doi: 10.1016/j.softx.2021.100723.
[38] F. Tuerlinckx, F. Rijmen, G. Verbeke, and P. De Boeck, “Statistical inference in generalized linear mixed models: A review,” *British Journal of Mathematical and Statistical Psychology*, vol. 59, no. 2, pp. 225–255, 2006, doi: 10.1348/000711005X79857.
[39] B. M. Bolker *et al.*, “Generalized linear mixed models: a practical guide for ecology and evolution,” *Trends in Ecology & Evolution*, vol. 24, no. 3, pp. 127–135, Mar. 2009, doi: 10.1016/j.tree.2008.10.008.
[40] S. Nakagawa and H. Schielzeth, “Repeatability for Gaussian and non-Gaussian data: a practical guide for biologists,” *Biological Reviews*, vol. 85, no. 4, pp. 935–956, 2010, doi: 10.1111/j.1469-185X.2010.00141.x.